JPE 19-2-6

https://doi.org/10.6113/JPE.2019.19.2.394
ISSN(Print): 1598-2092 / ISSN(Online): 2093-4718

Reduction of DC-Link Capacitance in Single-Phase Non-Isolated Onboard Battery Chargers

Hoang Vu Nguyen*, Sangmin Lee**, and Dong-Choon Lee†

†,*Department of Electrical Engineering, Yeungnam University, Gyeongsan, Korea
**Doosan Robotics Inc., Suwon, Korea

Abstract

This paper proposes a single-phase non-isolated onboard battery charger (OBC) for electric vehicles (EVs) that only uses small film capacitors at the DC-link of the AC-DC converter. In the proposed charger, an isolated DC-DC converter for low-voltage batteries is used as an active power decoupling (APD) circuit to absorb the ripple power when a high-voltage (HV) battery is charged. As a result, the DC-link capacitance in the AC-DC converter of the HV charging circuit can be significantly reduced without requiring any additional devices. In addition, some of the components of the proposed circuit are shared in common for the different operating modes among the AC-DC converter, LV charging circuit and active power filter. Therefore, the cost and volume of the onboard battery charger can be reduced. The effectiveness of the proposed topology has been verified by the simulation and experimental results.

Key words: Active filters, Plug-in electric vehicles, Single-phase chargers, Single-stage

I. INTRODUCTION

Interest in the charging technologies for plug-in hybrid EVs has been greatly increased due to the advent of more stringent regulations related to emissions, global warming, and resource constraints [1]-[3]. In plug-in EVs, the batteries are charged from the grid through an onboard battery charger (OBC) by connecting the EV to the grid. Since OBCs are installed in EVs, high efficiency and high power density are the main design consideration. By using wide band-gap power switches such as silicon carbide (SiC) and gallium nitride (GaN), a higher switching frequency and a higher efficiency can be achieved. Therefore, the power density of the OBC can be improved by shrinking the size of the passive components [4]. However, in single-phase battery chargers, there is an inherent ripple power component that fluctuates at double the grid frequency, which results in DC-link voltage ripple. Conventionally, to smoothen this low-frequency power ripple, bulky DC-link capacitor banks are used. This is the major barrier for high power density.

In order to reduce the DC-link capacitor banks in single-phase AC-DC converters, several active power decoupling (APD) circuits have been presented in the literature [5]-[11]. The fundamental principle is to use additional active circuits to absorb the ripple power at the DC-link. In [6] and [7], a symmetrical half-bridge circuit with a capacitor-split decoupling cell is used as a buffer to mitigate the ripple power and filtering switching ripple. However, active methods require additional components, which leads to increase the system complexity, cost and losses. In [4], [12] and [13], a sinusoidal current charging scheme was proposed, where a HV battery is charged by current with the ripple power frequency. However, this method can affect charging efficiency and its impact on lithium-ion batteries needs to be investigated further [14].

Meanwhile, with the development of EVs, there is a demand for multifunctional charging systems that can reduce the weight, volume, and cost of the charger. In EVs, a low-voltage (LV) battery is used to supply power for electrical equipment such as the lights, audio system, and ECUs [15]. Unlikely conventional vehicles which use an alternator, these LV batteries are charged from a high-voltage (HV) battery through an isolated DC-DC converter. Therefore, in order to achieve this goal, several multifunctional chargers were presented, where some of the switches and devices are utilized in common to minimize the circuit components [16]-[19]. In

Manuscript received Oct. 5, 2018; accepted Jan. 5, 2019
Recommended for publication by Associate Editor Jongbok Baek.
†Corresponding Author: dclee@yu.ac.kr
Tel: +82-53-810-2582, Fax: +82-53-810-4767, Yeungnam University
*Department of Electrical Engineering, Yeungnam University, Korea
**Doosan Robotics Inc., Korea

these circuits, by combining the AC-DC converter and the DC-DC converter, several switches are shared during HV and LV charging durations. However, these chargers still require bulky capacitor banks at the DC-link. In [20] and [21], an integration circuit composed of an active power filter and an LV battery charger was proposed to reduce the overall size of the converter. However, this charger can only operate with a unidirectional power flow. Moreover, in order to improve system efficiency and power density, a non-isolated OBC has been studied by eliminating the transformer, which reduces the volume and improves the efficiency of a charger. These non-isolated OBCs can satisfy the standards of conductive chargers for EVs (SAEJ1772) since the high-voltage battery is floated with the body ground of the vehicle [22]. Therefore, a multifunctional system based on a non-isolated OBC can be considered.

This paper proposes an improved LV charger for OBCs, where the isolated DC-DC converter is utilized as an active power decoupling circuit. When the OBC is connected to the grid, the proposed circuit can function as an active filter to eliminate low-frequency ripple power by sharing the switching devices with the AC-DC converter. As a result, small film capacitors can be employed instead of large capacitor banks or additional active power decoupling circuits. Therefore, the size and cost of the OBC are significantly reduced. In addition, this structure has an advantage which can implement in three different modes such as grid-to-vehicle (G2V), vehicle-to-grid (V2G), and HV-to-LV battery (H2L) modes. For G2V mode, the HV battery of an EV is charged from the grid. For the V2G mode, power is delivered to the grid from a HV battery. For the H2L mode, the charger is operated as a DC-DC converter to charge a LV battery from a HV battery. The feasibility of the proposed OBC is verified by simulation and experimental results.

II. Proposed Integrated Onboard Battery Charger

A. Configuration of the Proposed Onboard Battery Charger

The circuit configuration of the proposed dual functional circuit (DFC) is shown in Fig. 1, where the preliminary version was presented in [23]. It is composed of a symmetrical half-bridge circuit for the APD function and an isolated DC-DC converter for the LV charging circuit. A bidirectional buck-boost converter is utilized to manage the power flow between the HV battery and the DC-link. The APD circuit consists of one converter leg (S_5, S_6), two identical film capacitors with the same capacitance (C_{dc1}, C_{dc2}), and a small filter inductor (L_r). The LV charging circuit consists of the switches (S_5, S_6), two identical film capacitors (C_{dc1}, C_{dc2}), the diodes (D_1 to D_4), an output capacitor (C_{Lo}), an output inductor (L_{Lo}), and a transformer. The relay SW_2 is used for switching between the

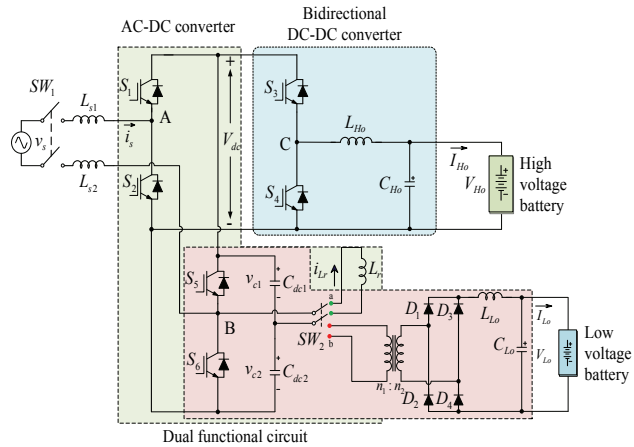

Fig. 1. Proposed OBC with a dual function circuit.

APD function and LV battery charging. When the OBC is operated in the G2V or V2G mode, the DFC is used as an active power filter to absorb the ripple power. While the EV is running, the DFC is operated as an LV charging circuit that charges the LV battery from the HV battery. In the proposed OBC, several of the components are utilized in common for the AC-DC converter with an active filter function and the LV charging circuit. Hence, by adding a small filter, APD capability is achieved without adding switching devices, gate drivers and heat sinks. In this circuit, the number of switching devices is the same as that of the conventional H-bridge AC-DC converter.

B. Proposed LV Battery Charger Circuit with Active Power Decoupling Function Headings

In Mode 1 (G2V) and Mode 2 (V2G), the DFC can work as an AC-DC converter with an APD function. The power flow of the OBC in Mode 1 and Mode 2 is shown in Fig. 2. A similar concept has been suggested in [24], [25], in which the dual active bridge DC-DC converter of the HV battery charger is used to provide the isolation between HV battery and LV battery. So, it is only acceptable for the two-stage battery charger. Also, in these circuits, the isolation between the LV battery and the DC link is not provided. The buck converter has to step-down the voltage from the DC-link to LV battery, leading to higher power losses due to the effect of the low duty cycle. Meanwhile, since the proposed HDC in this work is a part of the half-bridge DC-DC converter, the isolation and step-down ratio are provided by the existing transformer of LV charger. Therefore, this method is applicable to other single-stage or two-stage HV battery chargers. Furthermore, in this scheme, the number of switching devices for the AC-DC conversion stage is the same as that of the conventional full-bridge PWM converter, where one converter leg can be eliminated compared with the charger suggested in [23]-[25]. The DC link is comprised of two identical film capacitors connected in series, $C_{dc1} = C_{dc2} = C_f$, where its middle point is connected to one of the converter legs through the small filter inductor L_r. In order to decouple the ripple power component

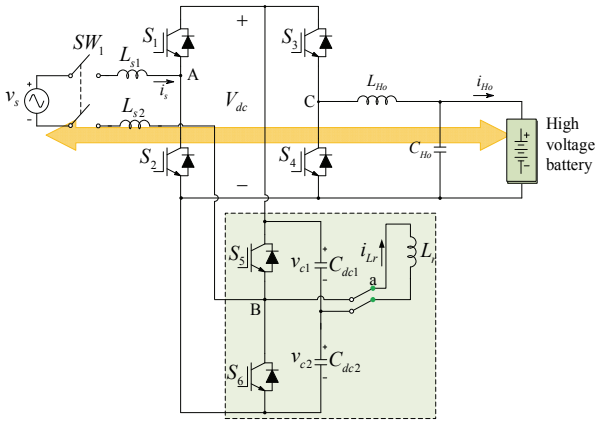

Fig. 2. Operation of a DFC in Mode 1 and Mode 2.

in single-phase onboard chargers, this inverter leg needs to be modulated in such a way that ripple power is absorbed by two DC-link film capacitors. Then the other converter leg is used to control the DC-link voltage and to keep the grid current sinusoidal. To do this, the upper and lower capacitor voltages $(v_{c1}$ and $v_{c2})$, which should be controlled to be sinusoidal with an offset value that is equal to a half of the DC-link voltage. These capacitor voltages can be expressed as:

$$v_{c1} = \frac{V_{dc}}{2} + \sqrt{2}V_c \sin(\omega t + \varphi) \tag{1}$$

$$v_{c2} = \frac{V_{dc}}{2} - \sqrt{2}V_c \sin(\omega t + \varphi), \tag{2}$$

where

$$V_c = \sqrt{\frac{\sqrt{(V_s I_s)^2 + (\omega V_s I_s^2)^2}}{2\omega C_f - \omega L_r (2\omega C_f)^2}} \tag{3}$$

and

$$\phi = -\frac{\pi}{4} \text{ or } \phi = \frac{3\pi}{4}. \tag{4}$$

Then the voltage references of C_{dc1} and C_{dc2} can be determined by (7) and (8). However, these values are highly dependent on the system parameters, which are difficult to determine exactly. To overcome this difficulty, closed-loop control was proposed in [7].

A control block diagram of an AC-DC converter with the APD function in Mode 1 is shown in Fig. 3. At first, the DC-link voltage is controlled by a PI controller. Then from the DC voltage controller, the grid current reference is obtained, where the PR controller is adopted to keep the grid current sinusoidal at a unity power factor as shown in Fig. 3(a). To achieve APD capability, the power ripple at the DC-link needs to be eliminated. A cascaded control loop is used to control the APD circuit. In the inner loop, the inductor current is regulated by a PI controller. In the outer loop, the PR controller is adopted to control the DC-link voltage ripple. The basic principle of the

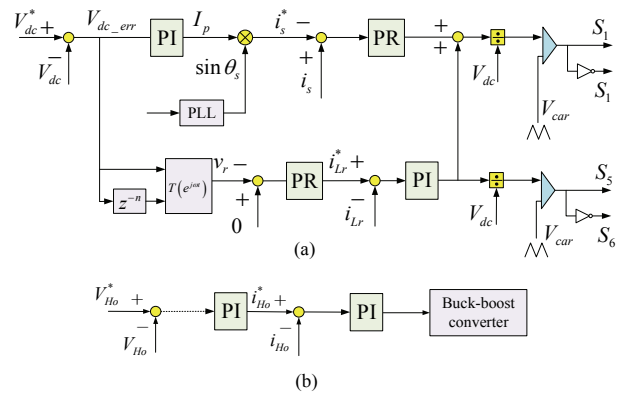

Fig. 3. Control block diagram of the proposed battery charger in Mode 1. (a) AC-DC converter and APD circuit. (b) Buck-boost converter.

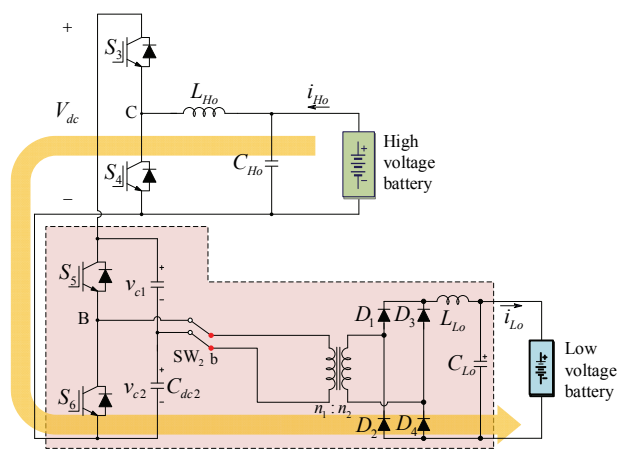

Fig. 4. LV charging operation in Mode 3.

APD circuit is to control the capacitor voltage as defined in (1) and (2), which only contains the fundamental frequency component. However, the DC-link voltage error is a second-order harmonic component. Therefore, it needs to be transformed into the fundamental frequency domain by the matrix given by

$$T(\omega t) = \begin{bmatrix} \cos(\omega t) & \sin(\omega t) \\ -\sin(\omega t) & \cos(\omega t) \end{bmatrix}. \tag{5}$$

Finally, the output of the APD controller is summed with that of the grid current controller, which produces the phase voltage reference for leg A.

Fig. 3(b) shows a control block diagram for charging a HV battery. The PI controller is used to regulate the battery current. In this case, the HV battery is assumed to be charged in the constant current-constant voltage (CC-CV) mode. In the V2G mode, the buck-boost converter is used to manage the HV battery power. The DC-link voltage and grid current are controlled by the AC-DC converter, in which the closed-loop control is also adopted. The controllers are the same as those of Fig. 3(a) except that the signs of the DC-link voltage and the grid current are reversed.

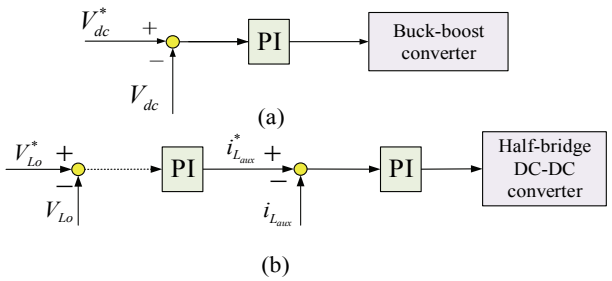

Fig. 5. Control block diagram of the proposed battery charger in Mode 3. (a) Buck-boost converter. (b) Half-bridge DC-DC converter.

In Mode 3 (H2L), the proposed DFC is operated as an isolated DC-DC converter to charge the LV battery. The power flow of the OBC in Mode 3 is shown in Fig. 4. In this case, the LV battery is charged from the HV battery through the buck-boost converter and the isolated DC-DC converter, where the control block diagram is shown in Fig. 5. The buck-boost converter can regulate the DC-link voltage with the PI controller, as shown in Fig. 5(a). Then the current and voltage of the LV battery are managed by the isolated DC-DC converter, as shown in Fig. 5(b).

III. Design Consideration and Comparative Analysis

A. Design of the Capacitors and Inductor for APD Circuit

The ripple power of the APD circuit is highest when the capacitor voltages are equal to a half of the DC-link voltage. Then the capacitance C_f of the filter capacitor is obtained as

$$C_f = \frac{4V_s I_s}{V_{dc}^2 \omega}. \tag{6}$$

Therefore, the equivalent DC-link capacitance C_{eq} is defined as

$$C_{eq} = \frac{C_f}{2} = \frac{2V_s I_s}{\omega V_{dc}^2} = \frac{2P_{in}}{\omega V_{dc}^2}, \tag{7}$$

where P_{in} is the input power. Considering the ripple power in L_s and L_r, for a 3.3-kW system, the equivalent DC-link capacitance is selected as 175μF and $C_f (= C_{dc1} = C_{dc2}) = 350\mu\text{F}$.

Meanwhile, for the conventional full-bridge AC-DC converter, the DC capacitance is given by [9]

$$C = \frac{P_{in}}{\omega V_{dc} \Delta V_{dc}}. \tag{8}$$

If the specified peak-to-peak ripple voltage ΔV_{DC} is set to 7 V, the required capacitance is about 3.5 mF.

Furthermore, to select the filter inductor L_r of the APD circuit, the cancelation coefficient α is defined as [26]

$$\alpha = \omega^2 L_r C_f, \tag{9}$$

where

$$L_r = \frac{\alpha}{\omega^2 C_f}. \tag{10}$$

In this work, α is chosen as 0.075. Then, the inductance L_r is selected as 1.5 mH.

B. Design of Capacitor and Inductor Filters for HV and LV batteries

To design the output filter of a DC-DC converter for a HV battery, it is assumed that the minimum operating voltage of the traction battery (V_{Ho}) is 200V. The filter inductance L_{Ho} is determined as [27]

$$L_{Ho} = \frac{V_{Ho}(V_{DC} - V_{Ho})}{\Delta I_{L_{Ho}} f_{sw} V_{DC}}, \tag{11}$$

where f_{sw} is the switching frequency, and $\Delta I_{L_{Ho}}$ is the inductor ripple current. In this work, the proposed circuit is operated at a switching frequency of 10 kHz and a maximum inductor current ripple of 3.3 A. Then the minimum value of L_{Ho} is calculated as 2.6 mH. In this system, a 3 mH inductor is selected.

When choosing the output capacitor (C_{Ho}), the following equation can be used to adjust the output capacitor values for a desired output voltage ripple (ΔV_{Ho}) [27]:

$$C_{Ho} = \frac{\Delta I_{L_{Ho}}}{8 f_{sw} \Delta V_{Ho}}. \tag{12}$$

If the maximum capacitor ripple voltage is 0.5 V, the minimum value of C_{Ho} is 82.5 μF. In this paper, a 100 μF film capacitor is selected.

When the proposed OBC is operated in the H2L mode, the LV battery is charged from a HV battery through the isolated DC-DC converter. This converter is designed to be able to control the output voltage in the range of 10 V to 24 V. Therefore, the turn ratio of the transformer is selected as 15:1. The power rating of the LV charger is designed to provide a maximum power of 1 kW. By (11) and (12), it is possible to determine the output inductor (L_{Lo}) and capacitor (C_{Lo}) of the LV charger. If the maximum inductor ripple current is 4 A and the battery ripple voltage is 0.04 V, the values of L_{Lo} and C_{Lo} are 150 μH and 200 μF, respectively.

C. Comparative Analysis

In this section, the cost, volume and efficiency of the proposed OBC are evaluated and compared with those of the conventional topology [19]. For a simple evaluation, only the costs and volumes of the switches, gating drivers, diodes, relay, capacitors, and inductors are taken into account [28]–[31]. The

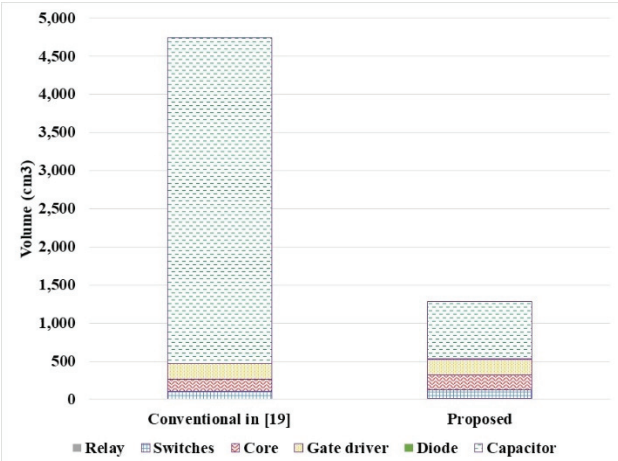

Fig. 6. Comparison of the volumes of two chargers.

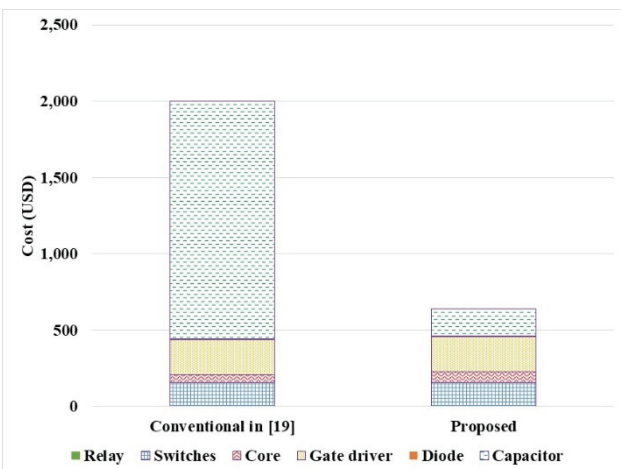

Fig. 7. Comparison of the costs of two chargers.

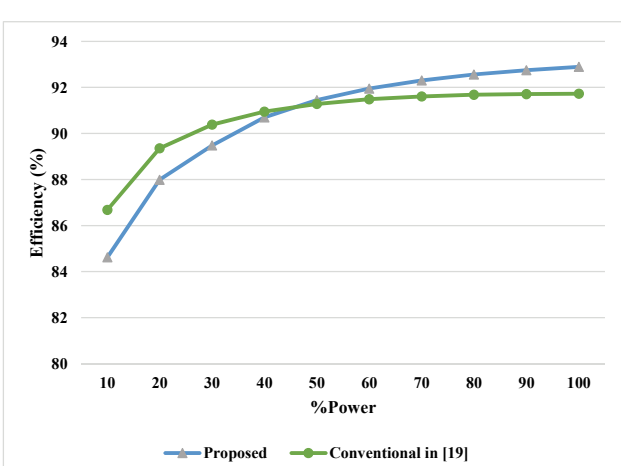

Fig. 8. Comparison of efficiencies in the G2V mode.

volume comparison is summarized in Fig. 6, where the overall volume of the proposed charger is decreased by 74.4% when compared with that of the conventional charger. In addition, with the proposed LV charger with the APD function, the overall cost of the proposed circuit is decreased by 67.8% due to a reduction of the DC-link capacitor, as shown in Fig. 7. The efficiency of the proposed topology in the G2V mode is shown in Fig. 8 and compared with that of the conventional converter. It can be seen that the proposed circuit can achieve a higher efficiency under the full load condition, where the peak efficiency is 92.89%. As the load power decreases, the efficiency drop is about 2% since the current stress of leg B is relatively high to achieve the APD capability.

TABLE I
PARAMETERS OF AN EV CHARGING SYSTEM

Parameters	Values
HV charger	3.3 kW
LV charger	1 kW
DC-link voltage	350 V
Grid voltage	110-V RMS
C_f	350 uF
L_r	1.5 mH
Transformer turn ratio	15:1
HV battery voltage	200-300 V
LV battery voltage	24 V
C_{aux}	100 uF
Switching frequency	10 kHz
L_{s1}, L_{s2}	1.5 mH
L_{Ho}	3 mH
C_{Ho}	100 uF
L_{Lo}	150 uH
C_{Lo}	200 uF

IV. SIMULATION RESULTS

To verify the validity of the proposed OBC, the PSIM simulation has been carried out for a 3.3-kW system. Table I lists the parameters of the simulation system.

Fig. 9 shows the operation of the OBC in Mode 1. In this mode, the proposed DFC is operated as an active filter to keep the constant DC-link voltage, where only small capacitors are used, as shown in Fig. 9(a). The grid current is controlled to be sinusoidal at unity power factor, as shown in Fig. 9(b). It can be seen that the current of leg B, i_B, is lower than the grid current even although one inverter leg is eliminated compared with the charger suggested in [23]–[25]. The closed-loop control is operated well so that the capacitor voltages are controlled as in (1) and (2), which are shown in Fig. 9(c).

Fig. 10 shows the operation of the buck-boost converter when the HV battery is charged with a constant current. It can be seen in Fig. 10(a) that the current is well regulated at 11A. The battery voltage is 300V, as shown in Fig. 10(b). Since the main objective of this research is to integrate the LV battery charger and APD circuit in an all-in-one system, a resistive load instead of real batteries is used, where the CC charging mode is performed for both HV and LV batteries.

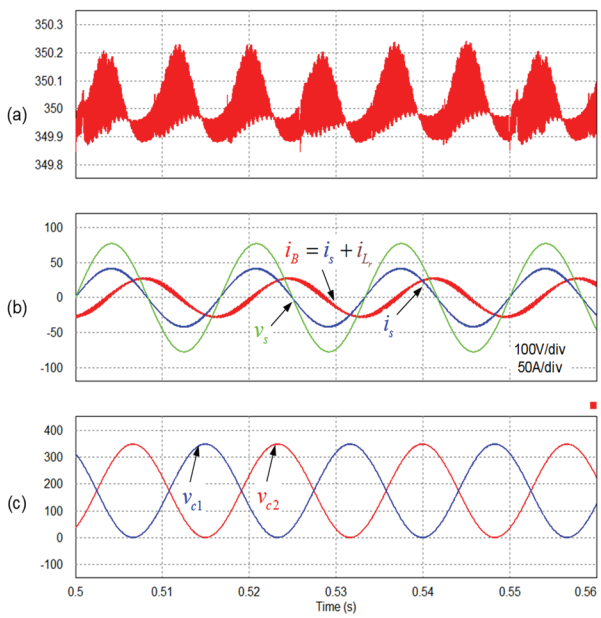

Fig. 9. Performance of the proposed OBC in Mode 1. (a) DC-link voltage. (b) Grid current, grid voltage, and phase B current. (c) Capacitor voltage.

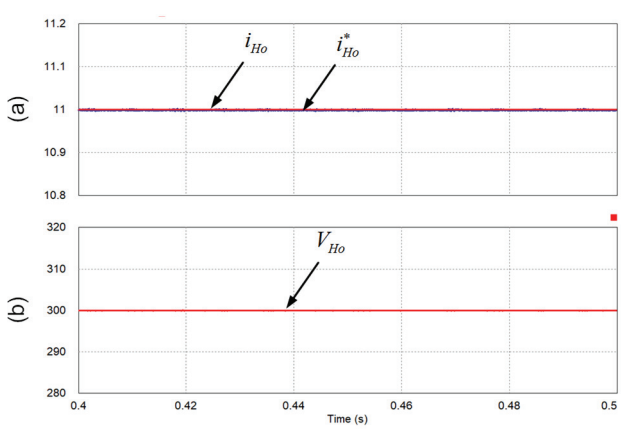

Fig. 10. Control performance of a DC-DC converter under a constant-current charging profile. (a) HV battery current. (b) HV battery voltage.

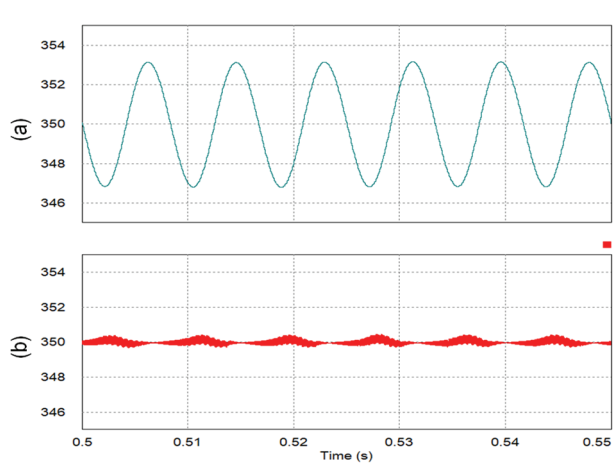

Fig. 11. Comparison of DC-link voltages. (a) With 3,500 μF DC-link capacitor. (b) With proposed method and 350 μF.

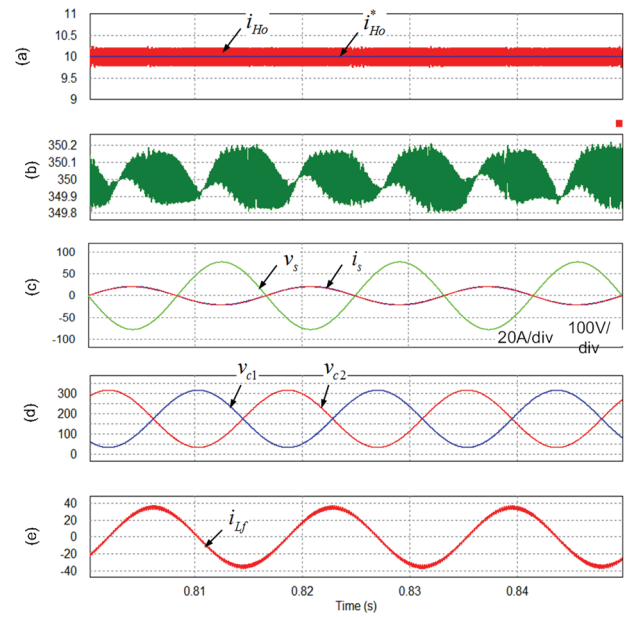

Fig. 12. Performance of the proposed OBC in Mode 2. (a) HV battery current (b) DC-link voltage. (c) Grid current and voltage. (d) Capacitor voltage. (e) Inductor current.

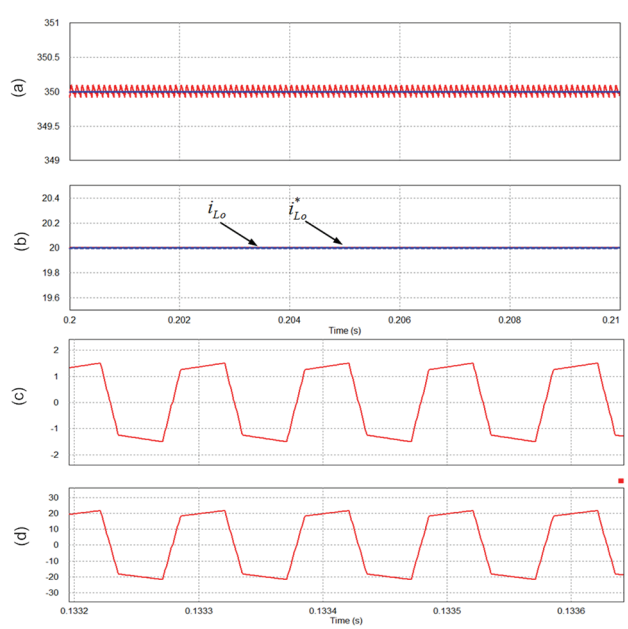

Fig. 13. Control performance of a battery charger in Mode 3. (a) DC-link voltage. (b) LV battery current. (c) Primary current of the transformer. (d) Secondary current of the transformer.

The control performance of the DC-link voltages for the conventional circuit with large capacitors and those of the proposed APD circuit are compared as shown in Fig. 11. In the conventional topology, a large DC-link capacitor of 3500 μF is needed to give the same DC-voltage.

Fig. 12 shows the performance of the OBC in Mode 2. During this mode, the HV battery provides the power to the grid, where the HV battery current is controlled by the DC-DC converter, as shown in Fig. 12(a). The DFC works as the DC-

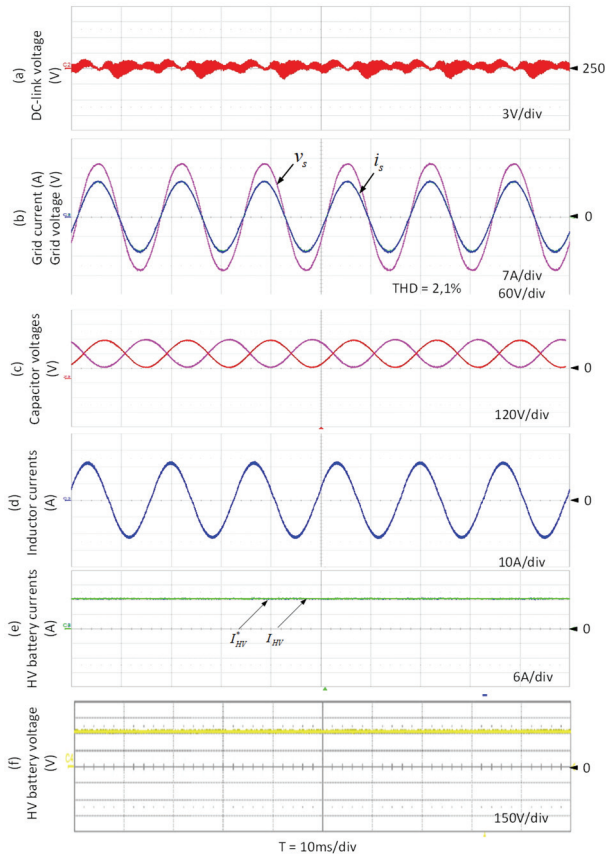

Fig. 14. Control of a battery charger in Mode 1. (a) DC-link voltage. (b) Input current and voltage. (c) Capacitor voltage. (d) Inductor current. (e) HV battery current. (f) HV battery voltage.

AC inverter to control the DC-link voltage and grid current, as shown in Fig. 12(b) and (c), respectively. The capacitor voltages and inductor current of the APD circuit are shown in Fig. 12(d) and (e), respectively.

The DFC acts as an LV charging circuit in Mode 3, whose performance is shown in Fig. 13. In this mode, the DC-link voltage is controlled by the buck-boost converter, as shown in Fig. 13(a). Then, the DFC works as the half-bridge DC-DC converter to control the LV battery current, as shown in Fig. 13(b). The primary and secondary currents of the transformer are shown in Fig. 13(c) and (d), respectively.

V. Experimental Results

In order to test the proposed charger, a 1-kW prototype was built in the laboratory. It is assumed that the power rating of the LV charger is 200W. The charger is controlled by a TMS320F28335 digital signal processor (DSP). The switching frequency is 10 kHz, where the gating signal is generated from a Xilinx FPGA device. The other parameters are the same as those of in Table I.

Fig. 14 shows experimental waveforms of the proposed OBC in Mode 1. The DC-link voltage is kept constant when the DFC works as the active filter to filter out the second-order

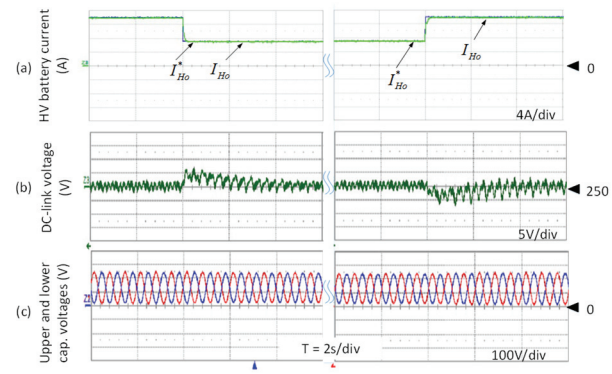

Fig. 15. Transient responses for stepwise load changes. (a) HV battery current. (b) DC-link voltage. (c) Capacitor voltage.

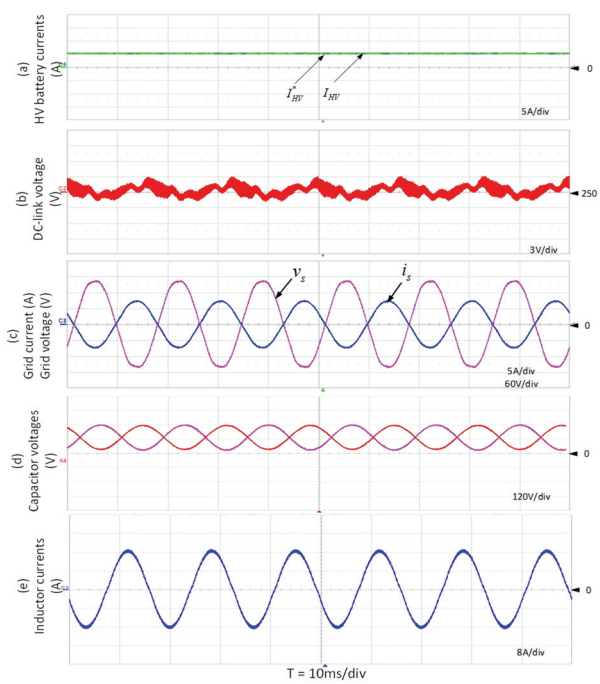

Fig. 16. Control performance of a battery charger in Mode 2. (a) HV battery current. (b) DC-link voltage. (c) Input current and voltage. (d) Capacitor voltage. (e) Inductor current.

ripple power, as shown in Fig. 14(a). The unity power factor operation is achieved, as shown in Fig. 14(b). Fig. 14(c) shows the capacitor voltages, which are opposite in phase and contain the offset component. The inductor current is shown in Fig. 14(d) and its peak value is about 20A. Fig. 14(e) and (f) show the control performance of the DC-DC converter under the constant-current charging condition. It can be seen that the current is well regulated at 12A and that the battery voltage is kept at 300 V.

Fig. 15 shows the performance of the OBC in the case of load variation. At the instance of the load change, the DC-link voltage fluctuation is kept below 5% compared with the average value.

The operation of the proposed charger in Mode 2 is shown in Fig. 16, where the discharged power of the HV battery is

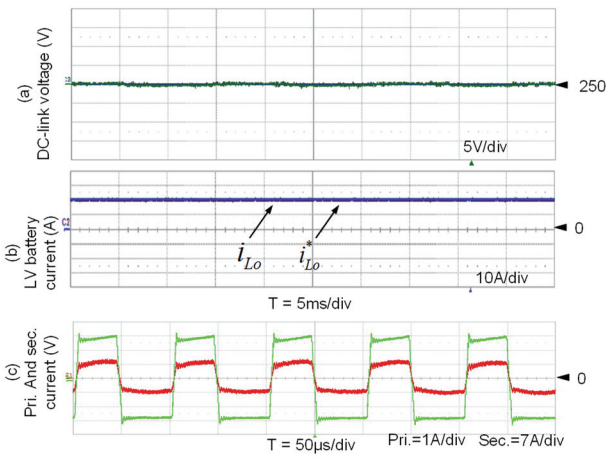

Fig. 17. Control performance of battery charger in H2L mode. (a) DC-link voltage. (b) LV battery current. (c) Primary and secondary current of the transformer.

regulated by the buck-boost converter. The DFC works as the inverter to control the DC-link voltage and grid current, where the APD is still achieved, as shown Fig. 16(a) - 16(c). The capacitor voltage and inductor current are also well regulated, as shown in Fig. 16 (d) and (e), respectively.

Fig. 17 shows the operation of a battery charger in Mode 3. The DC-link voltage is well controlled at 250V as shown in Fig. 17(a). The LV battery current is well controlled at the reference value, as shown in Fig. 17(b). The primary and secondary currents of the transformer are shown in Fig. 17(c), which are similar to those of the simulation results.

VI. Conclusions

A novel multifunctional battery charger for EVs has been proposed in this paper. The proposed OBC can implement a dual function that reduces the count of the circuit components. During the HV battery charging period, the vehicle is connected to the grid and the DFC is operated as an active power filter to absorb the second-order ripple power at the DC-link. During the LV battery charging period, the vehicle is running and the DFC is operated as an isolated DC-DC converter to charge the LV battery from the HV battery. With the proposed DFC, the LV battery charging circuit is utilized to achieve the APD function instead of bulky capacitor banks. Therefore, small film capacitors can be used without adding switches, a heat sink, or a corresponding gate circuit. As a result, for a 3.3-kW OBC, the volume and cost are decreased by 74.4% and 67.8%, when compared with the conventional method. The feasibility of the proposed OBC has been verified for a 1-kW prototype in the laboratory.

Acknowledgment

This research was supported by the National Research Foundation of Korea, under Grant NRF-2017R1A2A2A050 69629.

References

[1] C. C. Chan, A. Bouscayrol, and K. Chen, "Electric, hybrid, and fuel-cell vehicles: architectures and modeling," *IEEE Trans. Veh. Technol.*, Vol. 59, No. 2, pp. 589-598, Feb. 2010.

[2] Q. Qian, W. Sun, T. Zhang, and S. Lu, "A voltage-fed single-stage PFC full-bridge converter with asymmetric phase-shifted control for battery chargers," *J. Power Electron.*, Vol. 17, No. 1, pp. 31-40, Jan. 2017.

[3] M. Yilmaz and P. T. Krein, "Review of battery charger topologies, charging power levels, and infrastructure for plug-in electric and hybrid vehicles," *IEEE Trans. Power Electron.*, Vol. 28, No. 5, pp. 2151-2169, May 2013.

[4] L. Xue, Z. Shen, D. Boroyevich, P. Mattavelli, and D. Diaz, "Dual active bridge-based battery charger for plug-in hybrid electric vehicle with charging current containing low frequency ripple," *IEEE Trans. Power Electron.*, Vol. 30, No. 12, pp. 7299-7307, Dec. 2015.

[5] Y. Tang and F. Blaabjerg, "A component-minimized single-phase active power decoupling circuit with reduced current stress to semiconductor switches," *IEEE Trans. Power Electron.*, Vol. 30, No. 6, pp. 2905-2910, Jun. 2015.

[6] Y. Tang, F. Blaabjerg, and P. C. Loh, "Decoupling of fluctuating power in single-phase systems through a symmetrical half-bridge circuit," *IEEE Trans. Power Electron.*, Vol. 30, No. 4, pp. 1855-1865, Mar. 2015.

[7] Y. Tang, Z. Qin, F. Blaabjerg, and P. C. Loh, "A dual voltage control strategy for single-phase PWM converters with power decoupling function," *IEEE Trans. Power Electron.*, Vol. 30, No. 12, pp. 7060-7071, Dec. 2015.

[8] Y. Sun, Y. Liu, M. Su, W. Xiong, and J. Yang, "Review of active power decoupling topologies in single-phase systems," *IEEE Trans. Power Electron.*, Vol. 31, No. 7, pp. 4778-4794, Jul. 2016.

[9] R. Chen, Y. Liu, and F. Z. Peng, "DC capacitor-less inverter for single-phase power conversion with minimum voltage and current stress," *IEEE Trans. Power Electron.*, Vol. 30, No. 10, pp. 5499-5507, Oct. 2015.

[10] M. A. Vitorino, R. Wang, M. B. D. R. Correa, and D. Boroyevich, "Compensation of DC-link oscillation in single-phase-to-single-phase VSC/CSC and power density comparison," *IEEE Trans. Ind. Appl.*, Vol. 50, No. 3, pp. 2021-2028, May 2014.

[11] H. V. Nguyen, Y.-C. Jeung, and D.-C. Lee, "Battery charger with small DC-link capacitors for G2V applications," in *2016 IEEE International Conference on Sustainable Energy Technologies (ICSET)*, pp. 315-319, 2016.

[12] Siqi Li, J. Deng, and C. C. Mi, "Single-stage resonant battery charger with inherent power factor correction for electric vehicles," *IEEE Trans. Veh. Technol.*, Vol. 62, No. 9, pp. 4336-4344, Nov. 2013.

[13] K. M. Yoo, K. D. Kim, and J. Y. Lee, "Single-and three-phase PHEV onboard battery charger using small link capacitor," *IEEE Trans. Ind. Electron.*, Vol. 60, No. 8, pp. 3136-3144, 2013.

[14] A. J. Ruddell, A. G. Dutton, H. Wenzl, C. Ropeter, D. U. Sauer, J. Merten, C. Orfanogiannis, J. W. Twidell, P. Vezin, "Analysis of battery current microcycles in autonomous renewable energy systems," *J. Power Sources*, Vol. 112, No. 2, pp. 531-546, Nov. 2002.

[15] R. Hou, P. Magne, B. Bilgin, and A. Emadi, "A topological

evaluation of isolated DC/DC converters for auxiliary power modules in electrified vehicle applications," in *2015 IEEE Applied Power Electronics Conference and Exposition (APEC)*, pp. 1360-1366, 2015.

[16] Y.-J. Lee, A. Khaligh, and A. Emadi, "Advanced integrated bidirectional AC/DC and DC/DC converter for plug-in hybrid electric vehicles," *IEEE Trans. Veh. Technol.*, Vol. 58, No. 8, pp. 3970-3980, Oct. 2009.

[17] S. Dusmez and A. Khaligh, "A compact and integrated multifunctional power electronic interface for plug-in electric vehicles," *IEEE Trans. Power Electron.*, Vol. 28, No. 12, pp. 5690-5701, Dec. 2013.

[18] S. Kim and F. Kang, "Multifunctional on-board battery charger for plug-in electric vehicles," *IEEE Trans. Ind. Electron.*, Vol. 62, No. 6, pp. 3460-3472, Jun. 2014.

[19] J. G. Pinto, V. Monteiro, H. Goncalves, and J. L. Afonso, "Onboard reconfigurable battery charger for electric vehicles with traction-to-auxiliary mode," *IEEE Trans. Veh. Technol.*, Vol. 63, No. 3, pp. 1104-1116, Mar. 2014.

[20] R. Hou and A. Emadi, "Applied integrated active filter auxiliary power module for electrified vehicles with single-phase onboard chargers," *IEEE Trans. Power Electron.*, Vol. 32, No. 3, pp. 1860-1871, Mar. 2017.

[21] R. Hou and A. Emadi, "A primary full-integrated active filter auxiliary power module in electrified vehicles with single-phase onboard chargers," *IEEE Trans. Power Electron.*, Vol. 32, No. 11, pp. 8393-8405, Nov. 2017.

[22] D.-H. Kim, M.-J. Kim, and B.-K. Lee, "An integrated battery charger with high power density and efficiency for electric vehicles," *IEEE Trans. Power Electron.*, Vol. 32, No. 6, pp. 4553-4565, Jun. 2017.

[23] H. V. Nguyen and D. Lee, "Advanced single-phase onboard chargers with small DC-link capacitors," *in proc. of 2018 IEEE International Power Electronics and Application Conference and Exposition (PEAC)*, pp. 150-155, 2018.

[24] H. V. Nguyen and D.-C. Lee, "Single-phase multifunctional onboard battery chargers with active power decoupling capability," in *Proc. of 2018 IEEE Applied Power Electronics Conference and Exposition (APEC)*, pp. 3434-3439, 2018.

[25] H. V. Nguyen, D.-D. To, and D.-C. Lee, "Onboard battery chargers for plug-in electric vehicles with dual functional circuit for low-voltage battery charging and active power decoupling," *IEEE Access*, Vol. 6, No. 1, pp. 70212-70222, Oct. 2018.

[26] H. Li, K. Zhang, H. Zhao, S. Fan, and J. Xiong, "Active power decoupling for high-power single-phase PWM rectifiers," *IEEE Trans. Power Electron.*, Vol. 28, No. 3, pp. 1308-1319, Mar. 2013.

[27] B. Hauke, "Basic calculation of a buck converter's power stage," 2015.

[28] Mouser Electronics, "Products. Mouser Electronics." [Online]. Available: http://www.mouser.com/. [Accessed: 12-May-2018].

[29] Digi-Key Electronics., "Products. Digi-Key Electronics." [Online]. Available: http://www.digikey.com/. [Accessed: 12-May-2018].

[30] TDK Electronics, "Ferrite for Switching Power Supplies," 2011. [Online]. Available: https://www.tdk.co.jp.

[31] Semikron, "Products. Semikron." [Online]. Available: https://www.semikron.com. [Accessed: 12-May-2018].

Hoang Vu Nguyen was born in Can Tho, Vietnam. He received his B.S. degree in Electrical Engineering from Can Tho University, Can Tho, Vietnam, in 2012. He is presently working toward his Ph.D. degree in the Department of Electrical Engineering, Yeungnam University, Gyeongsan, Korea. Since 2013, he has been working as a Lecturer at the Can Tho University of Technology, Can Tho, Vietnam. His current research interests include AC-DC converters, DC-AC inverters, and electric vehicle battery chargers.

Sangmin Lee received his B.S. and M.S. degrees in Electrical Engineering from Yeungnam University, Gyeongsan, Korea, in 2015 and 2017, respectively. He is presently working at Doosan Robotics Co., Ltd., Suwon, Korea. His current research interests include modular DC-DC converters and machine control.

Dong-Choon Lee received his B.S., M.S. and Ph.D. degrees in Electrical Engineering from Seoul National University, Seoul, Korea, in 1985, 1987 and 1993, respectively. He was a Research Engineer for Daewoo Heavy Industry, Korea, from 1987 to 1988. He has been a faculty member in the Department of Electrical Engineering, Yeungnam University, Gyeongsan, Korea, since 1994. He was a Visiting Scholar in the Power Quality Laboratory, Texas A&M University, College Station, TX, USA, in 1998; the Electrical Drive Center, University of Nottingham, Nottingham, ENG, UK, in 2001; the Wisconsin Electric Machines and Power Electronics Consortium, University of Wisconsin, Madison, WI, USA, in 2004; and the FREEDM Systems Center, North Carolina State University, Raleigh, NC, USA, from September 2011 to August 2012. He served as the Editor-in-Chief of the Journal of Power Electronics of the Korean Institute of Power Electronics, from January 2015 to December 2017, where he is currently serving as the President. His current research interests include power converter design and control, renewable energy and grid connection, AC machine drives, and power quality.